Fizika Nizkikh Temperatur, 2010, v. 36, Nos. 10/11, p. 1228–1243

Observation of anisotropic effect of antiferromagnetic ordering on the superconducting gap in $ErNi_2B_2C$

N.L. Bobrov, V.N. Chernobay, Yu.G. Naidyuk, L.V. Tyutrina, and I.K. Yanson

B. Verkin Institute for Low Temperature Physics and Engineering of the National Academy of Sciences of Ukraine
47 Lenin Ave., Kharkov 61103, Ukraine
E-mail: bobrov@ilt.kharkov.ua

D.G. Naugle and K.D.D. Rathnayaka

Department of Physics Texas A&M University, College Station TX 77843-4242, USA

Received March 10, 2010

The point-contact spectra of the Andreev reflection dV/dI curves of the superconducting rare-earth nickel borocarbide $ErNi_2B_2C$ ($T_c \approx 11$ K) have been analyzed in the «one-gap» and «two-gap» approximations using the generalized Blonder–Tinkham–Klapwijk model and the Beloborod'ko model allowing for the pair-breaking effect of magnetic impurities. Experimental and calculated curves have been compared not only in shape, but in magnitude as well, which provide more reliable data for determining the temperature dependence of the energy gap (or superconducting order parameter) $\Delta(T)$. The anisotropic effect of antiferromagnetic ordering at $T_N \approx \approx 6$ K on the superconducting gap/order parameter has been determined: as the temperature is lowered, Δ decreases by $\sim 25\%$ in the *c*-direction and only by $\sim 4\%$ in the *ab*-plane. It is found that the pair-breaking parameter increases in the vicinity of the magnetic transitions, the increase being more pronounced in the *c*-direction. The efficiency of the models was tested for providing $\Delta(T)$ data for $ErNi_2B_2C$ from Andreev reflection spectra.

PACS: **74.45.+c** Proximity effects; Andreev reflection; SN and SNS junctions;
74.70.Dd Ternary, quaternary, and multinary compounds (including Chevrel phases, borocarbides, etc.).

Keywords: nickel borocarbides, point contacts, multiband superconductivity, superconducting gap, antiferromagnetic transition.

Introduction

Quaternary intermetallic nickel borocarbides (hereafter borocarbides) of the RNi_2B_2C type (R is a rare-earth element) attract special interest (see surveys [1,2,3] and further references) as they include compounds with rather high superconducting transition temperatures (up to $T_c \approx 17$ K, R = Lu) and compounds with different types of magnetic ordering that include states with commensurate and incommensurate spin-density waves.

Borocarbides have a body centered tetragonal crystalline structure with the ratio $c/a \sim 3$ [1,2]. They have a rather complex Fermi surface (FS) consisting of several sheets [4,5]. FS is anisotropic [1,2] and has two characteristic groups of electrons possessing different Fermi velocities v_F (this was mentioned in [6] from the de Haas-van Alphen experiments [7,8]). The T_c of borocarbides is determined not by the total density of states $N(E_F)$, but by the contribution to the density of states which is made by the slow electrons of the nodal regions [2]. In the normal state the transport properties of borocarbides, in particular their resistivity ρ, are practically isotropic [1,2] because they are related to the groups of electrons that have relatively high velocities v_F with lower anisotropy and are unrelated to the nodal points at the Fermi surface [2].

In RNi_2B_2C (R = Dy, Ho, Er, Tm) compounds the element R contains 4*f*-electrons with partially filled *f*-shells having a magnetic moment. As a result, T_c of these compounds is appreciably lower in comparison with nonmagnetic borocarbides (R = Y, Lu [1–3]). The object of this study, $ErNi_2B_2C$, undergoes a superconducting transition at $T_c \sim 11$ K [1–3] and two magnetic transitions below T_c, which do not destroy superconductivity. The AFM ordering occurs at the Neel temperature $T_N \sim 6$ K when the Er ions form a transverse-polarized incommensurate spin-density wave state [1–3]. The AFM ordering entails structural distortions and thus reduces the crystal symmetry from tetragonal to orthorhombic [9]. This magneto-elastic effect

is regarded as a structural Jahn–Teller transition [10]. The modulation wave vector of the spin-density waves is practically independent of temperature and is along the *a*-axis (direction [100]), or the equivalent *b*-axis (direction [010]), the spins being aligned along the *b*-axis or the *a*-axis, respectively. As the temperature lowers further, the compound changes into a weakly ferromagnetic (WFM) state with $T_{WFM} \sim 2.3$ K in which a spontaneous vortex lattice is formed [11].

To understand the features of the superconducting state in magnetic borocarbides, it is essential to have information about the superconducting gap Δ (magnitude, behavior, anisotropy, etc.) or the superconducting order parameter (OP). The investigations of the gap Δ in $ErNi_2B_2C$ [12–16] give $\Delta = 1.6$–1.82 meV. Its temperature dependence corresponds on the whole to the BCS theory. It is noted [13,14] that on a paramagnetic–AFM transition Δ decreases and the pair-breaking parameter Γ [17] reaches a maximum in the transition region. The authors [13] interpreted the results using the theory [18] which predicts a decrease in Δ due to spin-density wave gaps that open in some parts of the FS. On the other hand, the influence of the AFM transition on Δ was not observed in subsequent tunnel measurements on $ErNi_2B_2C$ [15].

Detailed point-contact (PC) spectra of the Andreev reflection in $ErNi_2B_2C$ in two principal crystallographic directions have been obtained in our recent study [19]. The analysis of these spectra shows that:

1. They are essentially anisotropic and their behavior differs qualitatively from that in $LuNi_2B_2C$.

2. The AFM ordering lowered the gap.

3. The two-gap model can be efficient at describing the experimental results.

However, the large (six) number of fitting parameters involved in the two-gap model casts some doubt on the uniqueness of results. On the other hand, it is quite appropriate to determine to what extent the one-gap approximation can account for the nontrivial behavior of the superconducting OP (gap) [19]. In this study we have also analyzed the one- and two-gap approximation within the Beloborod'ko (BB) model [19,20] allowing for the pair-breaking influence of magnetic ions and on the basis of the generalized Blonder–Tinkham–Klapwijk (GBTK) model [21] allowing for the Dynes pair-breaking parameter [17].

Experimental technique

Here we detail the experimental technique, which was described in [19] only briefly because of the space limitations. The PC measurements were made on $ErNi_2B_2C$ single crystals ($T_c \approx 11$ K) grown from the melt (Ames Laboratory, Prof. P. Canfield's group) and were similar to those used in [22]. The crystals were thin (0.1–0.2 mm) plates with the *c*-axis normal to the plane of the plate. The surface pretreatment was similar to that for $LuNi_2B_2C$ [23,24] (either by etching in a 5% nitric acid-alcohol solution or by of cleavage). The other electrode was a high-purity Ag rod or Ag wire of 0.15 mm in diameter. In the latter case the wire surface was pre-washed in concentrated nitric acid. The contact was made between the pretreated single crystal surface and the loop-shaped wire. The use of the wire loop as a damper improved the mechanical stability of the contacts and made it possible to measure the characteristics of one of the contacts (in the *ab*-plane) both on heating from 1.45 K to $T > 11$ K (normal state) and on subsequent cooling from the normal sate to the starting lowest temperature.

The temperature measurements were made using a continuous flow He cryostat (its analog is described in [25]). An insert was placed inside the cryostat, which made a PC by touching the sample surface with the silver electrode at helium temperature. The typical PC resistance varied from several to tens of Ohms. For more elaborate investigations, the PCs were selected, which had the highest possible «tunneling» characteristics seen as an intensive maximum in the $dV/dI(V)$ curve at $V = 0$ and the strongest nonlinearity corresponding to at least a 10% change in $dV/dI(V)$ in the interval ± 8 mV. On some contacts the $dV/dI(V)$ spectra were measured in the interval from $T_{\min} = 1.45$ K to temperatures 1–2 K higher than $T_c \approx$ ≈ 11 K. The results were quite reproducible irrespective of the resistance of a particular contact. Therefore, here we analyze the measurements on two contacts along the principal crystallographic directions — along the *c*-axis and in the *ab*-plane. The detailed series of the $dV/dI(V)$ spectra were obtained at approximately equal temperature intervals. 30 curves were taken at rising temperature and 34 curves were measured at lowering temperature in the *ab*-plane, while 49 curves were measured in the *c*-direction at rising temperature. The contacts remained stable during the whole period of measurement.

Results and discussion

The temperature series of $dV/dI(V)$ curves measured on two $ErNi_2B_2C$–Ag contacts in the *ab*-plane and along the *c*-axis are shown in Fig. 1.

Parameters characterizing the contacts and $ErNi_2B_2C$ are described in [19]. The most important of them is the PC size (diameter) estimated as $d_{ab} \approx 9.1$ nm, $d_c \approx 4.4$ nm for the corresponding directions (Fig. 1). The coherence length ξ in this compound increases from 15 to ~ 23 nm [26] when T increases from 3 K to 8 K, which satisfies the requirement $d < \xi$ for the theory [27].

For better visualization, some $dV/dI(V)$ curves of Fig. 1 were symmetrized and then scaled by dividing by $dV/dI(V)$ in the normal state at the lowest temperature and the bias interval ± 8 mV. They are shown in Fig. 2 along with the results (lines) of the one-gap calculation within the GBTK model [21]. The scaled curved are

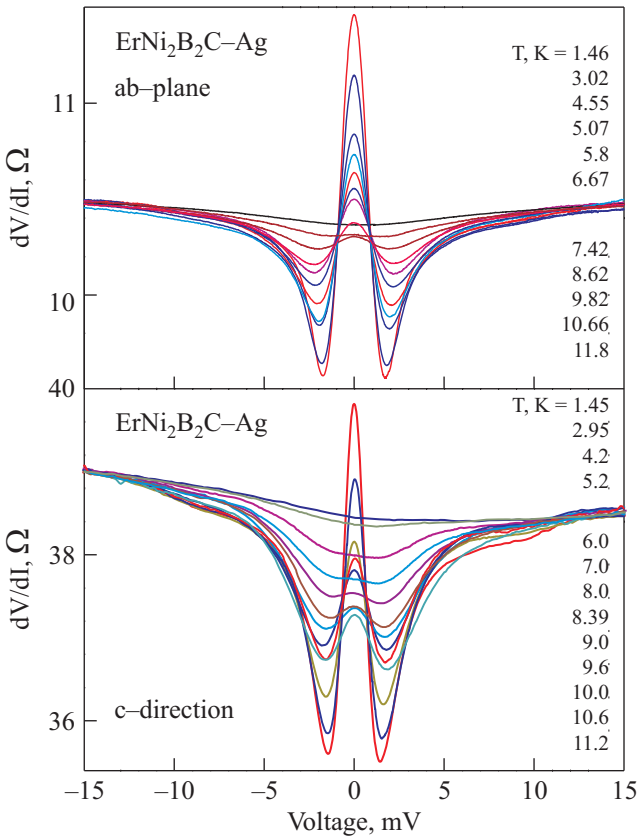

Fig. 1. Differential resistances of $ErNi_2B_2C$–Ag point contact formed in two principal directions at different temperatures. To avoid overloading, only a few of the curves are shown.

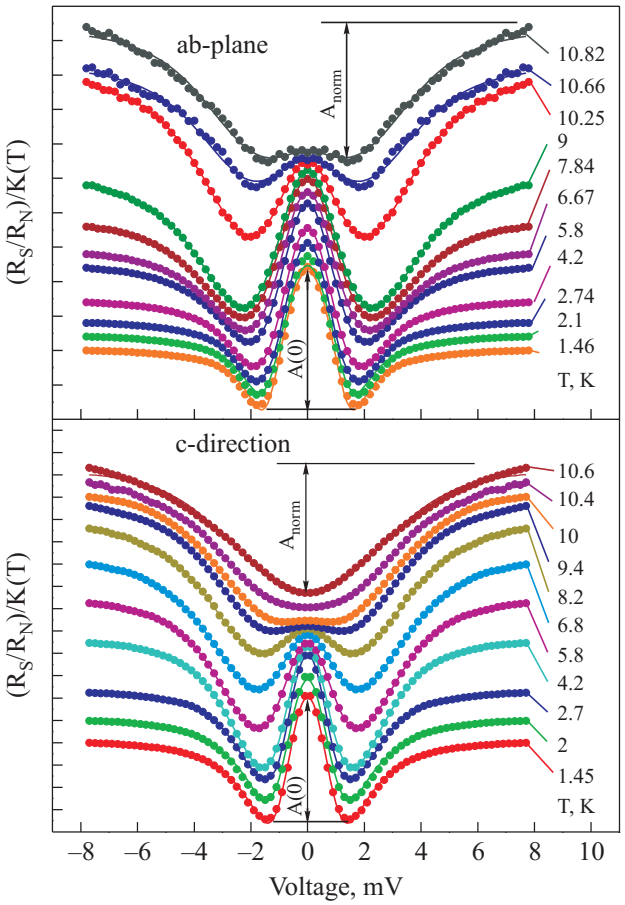

Fig. 2. Symmetrized curves of Fig. 1 normalized to the normal state at different temperatures. Points show experimental data. Lines are theoretical one-gap GBTK calculation. For visualization, all the curves are reduced to the same amplitude ($A(0) = A_{norm}$, see the text).

reduced to equal amplitude $A_{norm} = A(T)/M(T)$. Here $M(T) = A(T)/A(0)$, is a coefficient, where $A(T)$ is the amplitude at the temperature T. $A(0)$ is the amplitude of the curve normalized to the normal state at the lowest temperature in the bias interval ± 8 mV ($A_{norm} = A(0)$). Note that the smooth jump-free dependence $M(T)$ in the *ab*-plane and *c*-direction (Fig. 3) is indicative of the temperature stability of the point contacts.

Of interest is the unusual temperature dependence of the distance between the minima in dV/dI of the $ErNi_2B_2C$–Ag point contact (Fig. 4). It differs drastically from the corresponding dependence in dV/dI of a $ErNi_2B_2C$–Ag point contact having a similar tunneling parameter Z [23,24]. It is known that at low temperatures the half-distance between the minima in the $dV/dI(V)$ curve of high-tunneling ($Z \sim 1$ SN point contacts correlates quite well the superconducting energy gap)*. It should be noted that in the $ErNi_2B_2C$–Ag PC the two-minima structure of the dV/dI curve persists up to T_c in the *ab*-plane and 0.95 T_c in the *c*-direction. This is typical of tunnel contacts (e.g., [28]) and rather unusual in PCs, where the Andreev reflection is important and the tunnel parameter is $Z < 1(0.8)$.

Besides, there is another feature in the $ErNi_2B_2C$ spectra that is unobservable in $LuNi_2B_2C$: the distance between the minima in the dV/dI curve increases with temperature up to a maximum slightly above the temperature of the AFM transition. It is reasonable to attribute this behavior to the magnetic transition in $ErNi_2B_2C$. Such transitions are absent in $LuNi_2B_2C$.

It is also important that the local critical temperature in the investigated PCs (at which the main minimum disappears from the dV/dI curve) practically coincides with

* Even at the lowest temperature the interminima half-distance can correspond to the OP only when the broadening parameter γ [20] or Γ [17] is zero and the tunneling parameter Z is non-zero. Besides, the OP can vary in different regions of the Fermi surface e.q., due to anisotropy. There is no reason to expect that the interminima half-distance would coincide with the OP averaged over the Fermi surface. Therefore, it is expedient to calculate the temperature dependence of the averaged OP from the fitting results for the theoretical and experimental curves.

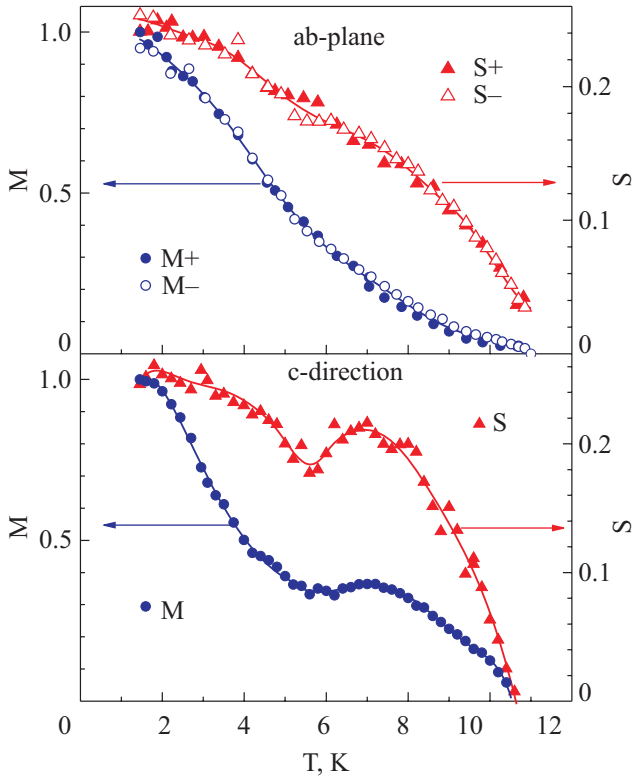

Fig. 3. Temperature dependencies of amplitude coefficients $M(T)$ obtained from the plots in Fig. 2 and scaling factors S calculated in the one-OP BB approximation and characterizing the intensity of experimental curves in comparison with theoretical one (see Figs. 11,12) in the *ab*-plane and the *c*-direction. Here and in the subsequent figures the measurements in the *ab*-plane are marked with solid symbols (rising temperature, +) and empty symbols (subsequent cooling, –). For visualization, a polynomial fit is drawn through the points.

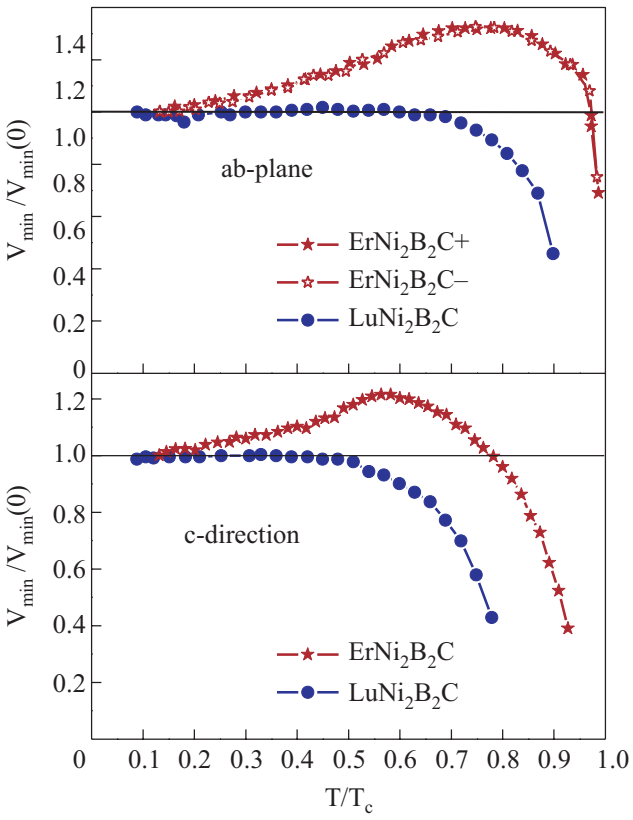

Fig. 4. The temperature dependence of the interminima distance normalized to the lowest-temperature value for the $ErNi_2B_2C$–Ag (Fig. 1) and $LuNi_2B_2C$–Ag [23] point contacts having similar tunnel parameters: $Z^{ab}_{Er} = 0.77$, $Z^{ab}_{Lu} = 0.7$, $Z^{c}_{Er} = 0.6$, $Z^{c}_{Lu} = 0.55$.

T_c of the crystal, which suggests that the properties of the material remain unaltered in the contact.

As is mentioned in the introduction, experimental data were analyzed in the one- and two gap approximations using two models.

1. The traditional GBTK model [21], which includes the broadening parameter Γ [17] characterizing inelastic pair-breaking processes.

2. The BB model [20] which introduces the pair-breaking parameter γ to account for the finite lifetime of Cooper pairs due to the pair-breaking action of (disordered) magnetic moments (in our case the Er ions possessing a magnetic moment).

The terms «energy gap» (GBTK model [21]) and «order parameter» [20] used in this model are of equivalent physical sense (see the detailed discussion in [20], p. 014512-3 and are therefore denoted identically with Δ. This, however, does not refer to the term «energy gap Δ_0» in the BB model [20] which differentiates the superconducting order parameter Δ and the energy gap Δ_0 [20]. The energy gap Δ_0 and the order parameter Δ are related as

$$\Delta_0 = \Delta(1-\gamma^{2/3})^{3/2} \qquad (1)$$

Here $\gamma = 1/\tau_s\Delta$ is the pair-breaking parameter, τ_s is the electron mean free time under spin–flip scattering. When this scattering is absent, τ_s tends to infinity and the equation describing the current-voltage characteristics (IVCs) [20] coincides with the corresponding equation of the classical BTK theory [27]. The equations describing the IVCs of PCs within this model are presented in [20,24].

One-gap approximation

The calculation technique of the most popular GBTK model minimizing the rms deviations F between the shapes of experimental and theoretical curves (see [24], Fig. 3) faces a certain problem: when the magnitudes of Γ and the gap Δ become comparable, the error curve for Δ has no distinct minimum, which is most typical of the *c*-direction (see Appendix, Fig. 18).

Note that in this comparison of the theoretical and experimental curves the parameter F characterizes only

the degree of their discrepancy in shape, while the distinctions in intensity are compensated using a scaling factor $S = (dV/dI)_{\text{exp}} / (dV/dT)_{\text{theor}}$. The scaling factor S, which characterizes the intensity ratio between experimental and theoretical curves, must be equal to 1. Sometimes this requirement of the GBTK model is violated and we have $S \neq 1$. Such factors and the ways of their selection are considered in Appendix B.

Calculation in GBTK and BB models with fixed S

The dependencies $\Delta(T)$ in the *ab*-plane and *c*-direction calculated with properly chosen *S*-factors are shown in Fig. 5.

Table 1 contains $\Delta(0)$ estimates (bold type) for both directions obtained with proper *S*-factors. Also, it includes GBTK data ($\Delta(0)$) for the maximum ($S = 1$) and minimum ($S = 0.25$) possible cases. Such S values appear because in this model the error in F changes only slightly when S deviates from its proper value (Figs. 18, 20).

Note that in the *ab*-plane the relation $2\Delta / kT_c = 3.52$ agrees with the BCS theory at $S = 0.31$ (our proper selection). In the *c*-direction the BCS relation $2\Delta / kT_c = 3.53$ ($\Delta(0)$) = 1.62 meV in the PM region is achieved at ($S = 0$. In this case the error in F increases only slightly, see Fig. 20,*b*).

Table 1. Superconducting energy gaps (GBTK) or OP_S (BB) Δ at different scaling factors S in the *ab*-plane and *c*-direction.

S	Direction, Face	GBTK		BB	
		$\Delta(0)$	$2\Delta / kT_c$	$\Delta(0)$	$2\Delta / kT_c$
0.25	ab,PM	1.8	3.76	1.95	4.08
	c,PM	2.17	4.73	2.36	5.14
0.31	**ab,PM**	**1.68**	**3.52**	—	—
0.65	**c,PM**	**1.48**	**3.23**	—	—
1	*ab*,PM	1.03	2.15	—	—
	c,PM	1.23	2.68	—	—

The calculation in the BB model gives $2\Delta / kT_c = 4$–5. This correlates with the tunnel investigation on nonmagnetic YNi_2B_2C, in which $2\Delta / kT_c = 5.2$ for the maximum gap (see [29], Fig. 6).

The critical temperature extrapolated to the paramagnetic region of the BCS curve is close to the values of the bulk compound $T_c = 10.64$ K (*c*-direction) and $T_c =$ = 11.1 K (*ab*-plane). At the same time at the AFM–PM transition the growth of Δ is essentially dependent on the direction. According to the BCS extrapolation, Δ increases by 25–28% in the *c*-direction and only by 4–5% in the *ab*-plane. Proceeding from the magnetic structure of ground-state $ErNi_2B_2C$ [1], this anisotropic influence of the magnetic transition on Δ can be attributed to orientationally-dependent spin-density waves. The AFM incommensurate ordering below the Neel temperature induces spin-density waves whose propagation vector **q** is in the *ab*-plane. Such waves reduce the superconducting gap for the electrons having the wave vector **k** perpendicular to the vector **q**, i.e., for the *c*-direction, due to the pair-breaking exchange field [30,31]. The same approach was used to interpret the anisotropy of the superconducting energy gap in the AFM heavy-fermion URu_2Si_2 compound [32]. The anisotropic effect of spin-density waves is also evident in the behavior of the parameter M (see Fig. 3), which has an extremum only in the *c*-direction. It is important that M characterizes the «gap minima» intensity of the original dV/dI spectra and is unrelated to any theoretical model.

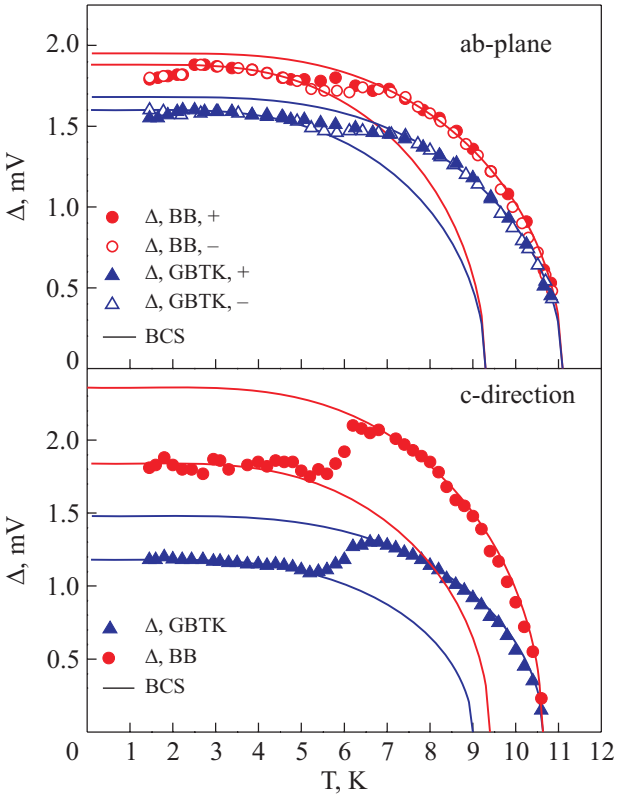

Fig. 5. Temperature dependencies of gaps (GBTK triangles) and OP_S (BB circles) calculated for the best-selected scaling factors S (Fig. 20.) for the PC in Fig. 1. Solid lines are BCS extrapolations.

The effect of spin fluctuations and the AFM molecular field on the superconducting gap is determined by the sum rule [33]. Their competition dictates whether the AFM phase will enhance or suppress the pair-breaking processes below T_N. The temperature dependence of the superconducting gap was calculated within the Chi–Nagi model [34] (Fig. 3 in [33]). In the paramagnetic region the superconducting gap follows the BCS dependence and in the AFM region (below T_N) its behavior is determined by the interaction between the temperature-dependent AFM molecular field and the spin-fluctuation scattering of conduc-

tion electrons at both magnetic rare-earth ions and nonmagnetic impurities. The molecular field opens AFM gaps in the some parts of the FS and destroys the superconducting gaps in them. Nonmagnetic impurities have no effect on the BCS states of a *s*-wave superconductor, but they attenuate the AFM field effect suppressing the pairing states of charge-density or spin-density waves. The degree of suppression of the superconducting gap is dependent on the single crystal perfection — elastic scattering assists in restoring superconductivity.

The temperature dependence of the energy gap $\Delta_0 = \Delta(1-\gamma^{2/3})^{3/2}$ (Fig. 6) can be obtained clearly within the BB model [20] as well. The BCS extrapolations on changing to gapless superconductivity in the AFM (6.6 K) and PM (9.3–9.6 K) regions correlate well in both direction with the BCS extrapolations of T_c for the OPs in these regions (Fig. 5). As in the OP case, the gap increases on changing to the PM state in the *c*-direction and exhibits a monotonic dependence in the *ab*-plane.

Note that the results of this study and [19] (decreasing OPs/gaps in the AFM region) correlate with the temperature dependencies of the coherence length, the penetration depth and the critical magnetic fields measured in single crystalline $ErNi_2B_2C$ which has features near T_N: an *N*-shaped curve of the coherence length and a local minimum in the penetration depth ([35], Fig. 1). There is also indirect evidence for the anisotropy of Δ which is based on measurements of the anisotropy of the upper critical magnetic field H_{c2} (it is known that $H_{c2} \sim \xi^{-2} \sim \Delta^2$). A 3D fourfold modulation of the upper critical field H_{c2} was measured in the field $\mathbf{H} \perp \mathbf{c}$ at $T = 2$ K as a function of the direction in the *ab*-plane (see [35], Fig. 4, insert). Its shape is similar to the anisotropic function of the superconducting energy gap in the model proposed in [36]. Note a distinct peak at T_N in the dependence $H_{c2}(T)$ in the field along the *c*-direction (Fig. 2 in [35]), which indicates indirectly that the AFM transition reduces the superconducting gap.

Figures 7 and 8 illustrate the pair-breaking parameters Γ and γ reduced to the same dimensionality: γ is compared with Γ/Δ and Γ with $\gamma\Delta$. The dependencies have features near the Neel temperature — a maximum in the *c*-direction and a smeared shoulder in the *ab*-plane. In the *c*-direction the pair-breaking parameter increases slightly near the transition to weak ferromagnetism (~ 2 K). In the *ab*-plane such increase is hard to identify because of the scatter of experimental points.

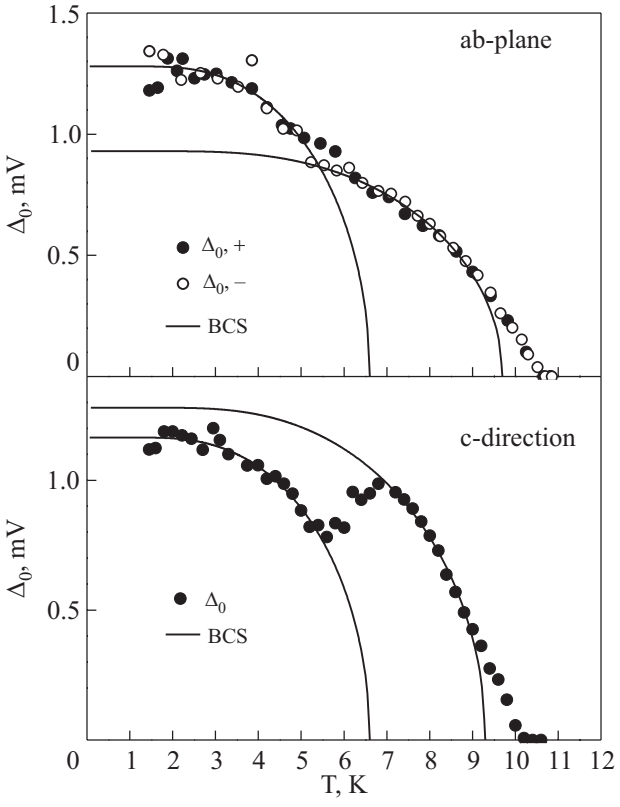

Fig. 6. The temperature dependencies of the BB calculated gap $\Delta_0 = \Delta(1-\gamma^{2/3})^{3/2}$ for the $ErNi_2B_2C$–Ag PC in the *ab*-plane and the *c*-direction. Solid lines are BCS extrapolations.

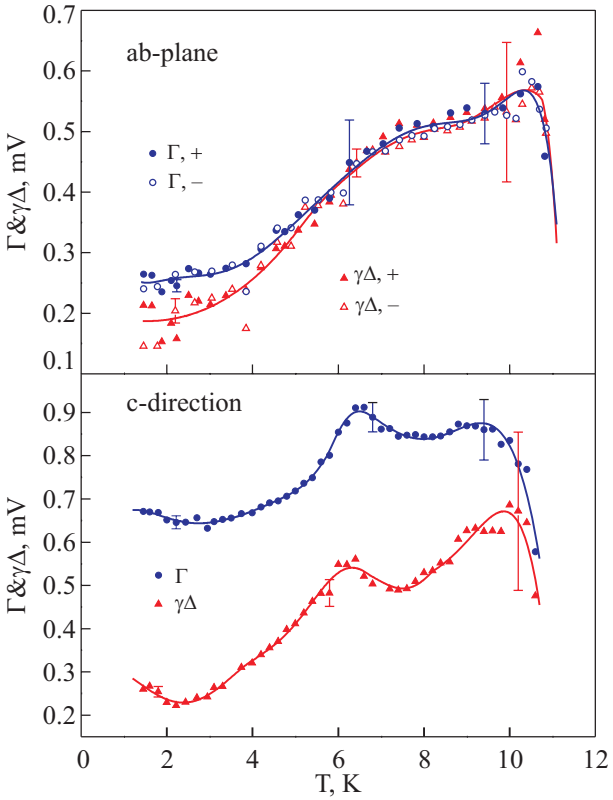

Fig. 7. Temperature dependencies of broadening parameters Γ and pair-breaking parameters γ reduced to the same units for the $ErNi_2B_2C$–Ag PC in the *ab*-plane and the *c*-direction. Error bars represent 5% deviations Δ from the minimum at curve of rms deviations of the shape of the theoretical curve from experimental one (see Fig. 18). Since $S = \text{const}$ was obtained by selecting the broadening (pair-breaking) parameter, a comparatively slight deviation of the points from the polynomial fit, the real deviation is much smaller.

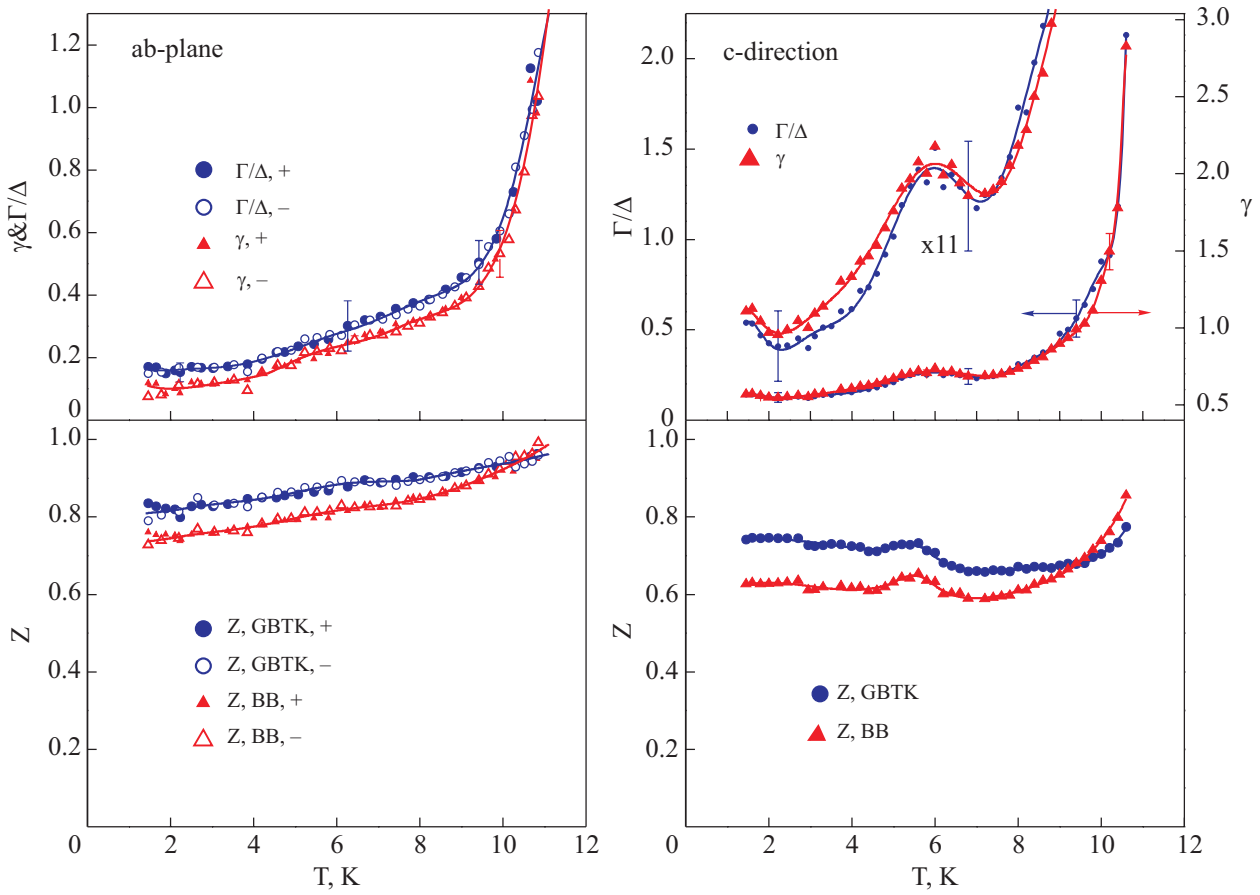

Fig. 8. Temperature dependencies of the pair-breaking parameter γ and the relative broadening parameter Γ/Δ (upper pictures) in comparison with the temperature dependencies of the tunnel parameter Z (lower pictures) for the $ErNi_2B_2C$–Ag PC in the *ab*-plane and the *c*-direction. The dependencies $\gamma(T)$ and $\Gamma/\Delta(T)$ are shown on an enlarged scale in the *c*-direction to visualize the maximum near the magnetic transition. The error bars are found as in Fig. 7.

There is a certain correlation between the pair-breaking parameter γ (hence, increasing scattering of superconducting electrons) and the tunneling parameter Z characterizing the potential barrier or the scattering at the NS boundary (see Fig. 8). Thus, the parameter Z may account for both the elastic scattering intensity and the spin–flip scattering. It is likely that the growth of these parameters near the AFM transition is more evident in the *c*-direction because of the anisotropic influence of the spin-density waves. On approaching T_c, γ and Z increase in both the *ab*-plane and the *c*-direction.

Calculation with a varying S-factor (BB model)

Note that the use of a fixed S in the BB model reduced the quality of fitting of theoretical to experimental curves. The reasons for such reduction in quality are considered in Appendix B. The temperature dependencies of OPs having freely varying S factors are shown in Fig. 9 for the *ab*-plane and *c*-direction (two-gap approximation with free S was used in [19]).

In both directions the OPs deviate from the BCS curve on approaching T_c (at $T \sim 10$ K) and turn zero at T_c of the contact. The critical temperature obtained for these parameters through a BCS extrapolation is $T_c = 11.9$ K in both directions. The temperature dependencies of the scaling factors S (Fig. 3) correlate in shape with those of the amplitude coefficients $M(T)$. Such temperature dependencies are due to the density of states curve in this model which differs from the BCS dependence (see the Appendix), as well as to the two-gap character of superconductivity in this compound whose OPs have significantly different magnitudes in the paramagnetic region (detailed in the following section).

Finally, Fig. 10 illustrates the temperature dependencies of the pair-breaking parameter γ. On the whole, they are similar to the temperature dependencies of the pair-breaking parameters for a large OP in the two-gap approximation [19] and differ considerably from the corresponding dependencies in the one-gap approximation obtained with a fixed scaling factor (Fig. 8), which is particularly evident in the high-temperature region. This may be because in the latter case we try to hold the scaling factor

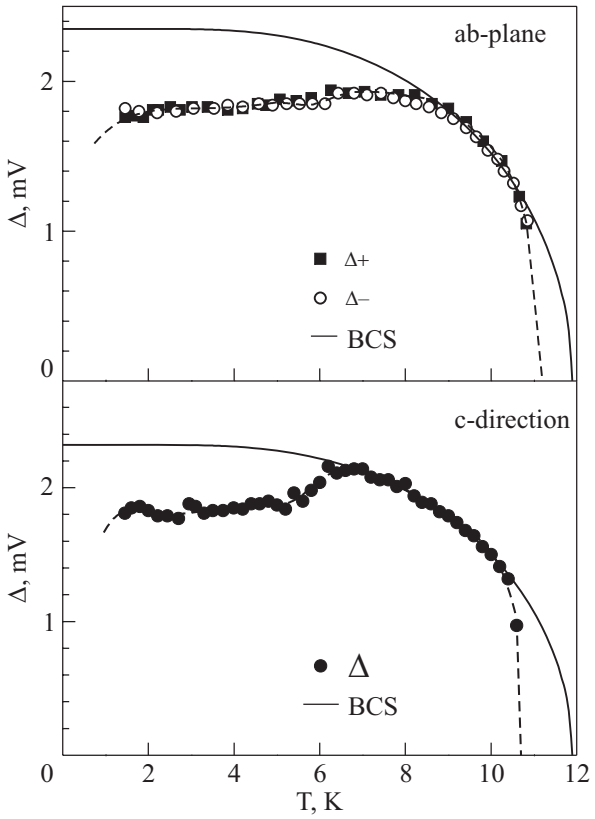

Fig. 9. Temperature dependencies calculated in the one OP approximation (BB model [20]) with $S \neq$ const. Solid lines are BCS extrapolations.

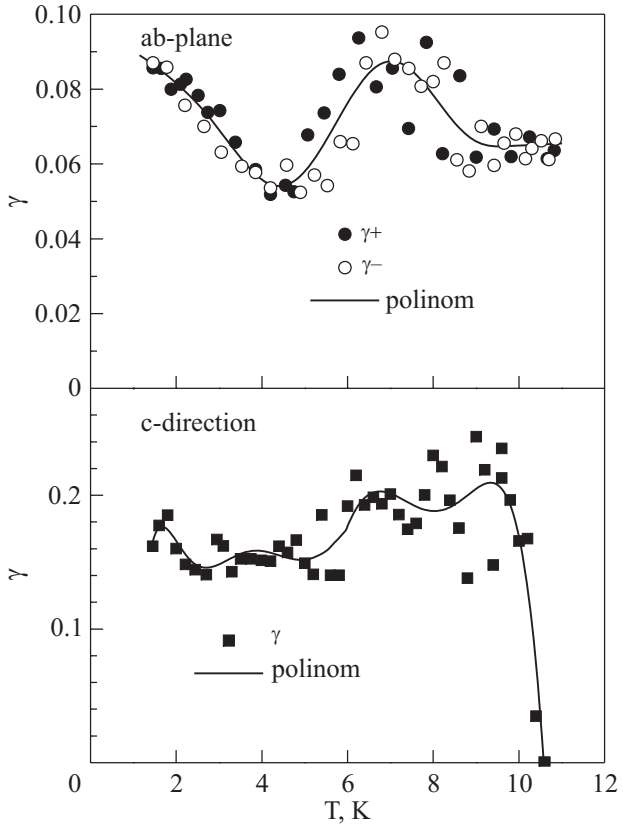

Fig. 10. Temperature dependencies of pair-breaking parameters γ in the one OP approximation with $S \neq$ const.

invariable at the expense of a certain departure from coincidence of the shapes of experimental and theoretical curves. In the vicinity of magnetic transitions pair-breaking parameters also increase in both *ab*-plane and *c*-direction.

Thus, the behavior of OPs and other parameters estimated in the one-gap approximation within the BB model with a free factor S is similar qualitatively to the results obtained in the two-gap approximation [19].

Two-gap approximation

The two-gap approximation assumes that the total conductivity is a superposition of conductivities from two region (bands) of the FS with corresponding gaps. This can be expressed for dV/dI as

$$\frac{dV}{dI} = \frac{S}{\frac{dI}{dV}(\Delta_1, \gamma_1, Z)K + \frac{dI}{dV}(\Delta_2, \gamma_2, Z)(1-K)}. \quad (2)$$

Here the coefficient K accounts for the contribution to the conductivity from the FS region with a smaller gap Δ_1, Z is the tunnel parameter, S is the scaling factor characterizing the intensity ratio of the experimental and theoretical curves, like in the one-gap approximation. This expression was used to fit experimental curves and to derive the parameters $\Delta_{1,2}$, $\Gamma_{1,2}$ (or $\gamma_{1,2}$), Z, S and K. The calculation technique is detailed in [24], Appendix.

The average gap is found from the expression

$$\Delta_{\text{aver}} = \Delta_1 K + \Delta_2 (1-K). \quad (3)$$

GBTK model

The temperature dependencies of the larger, smaller and the average gaps obtained in the two-gap approximation within the GBTK model with a fixed contribution K are shown in Fig. 11 (also see Appendix B).

Although K is fixed, the critical temperatures obtained through a BCS extrapolation are different for the larger and smaller gaps in the PM region, which may point to the two-gap character of superconductivity with a weak interband scattering. Such behavior is impossible in the case of ordinary OP anisotropy where these is only one critical temperature, according to Pokrovsky's theorem [37,38]. Besides, BCS extrapolation can be employed to estimate T_c in the AFM region for the larger gap in the *ab*-plane and for the smaller one in the *c*-direction. The temperature dependencies of the broadening parameters Γ are illustrated in Fig. 12. In the AFM region $\Gamma_1 > \Gamma_2$ in the *ab*-plane and $\Gamma_1 \sim \Gamma_2$ in the *c*-direction. The comparison with the one-gap calculation (Fig. 7) shows that the shapes of the curves in Fig. 7 are closer to Γ_2, i.e., the smearing of the

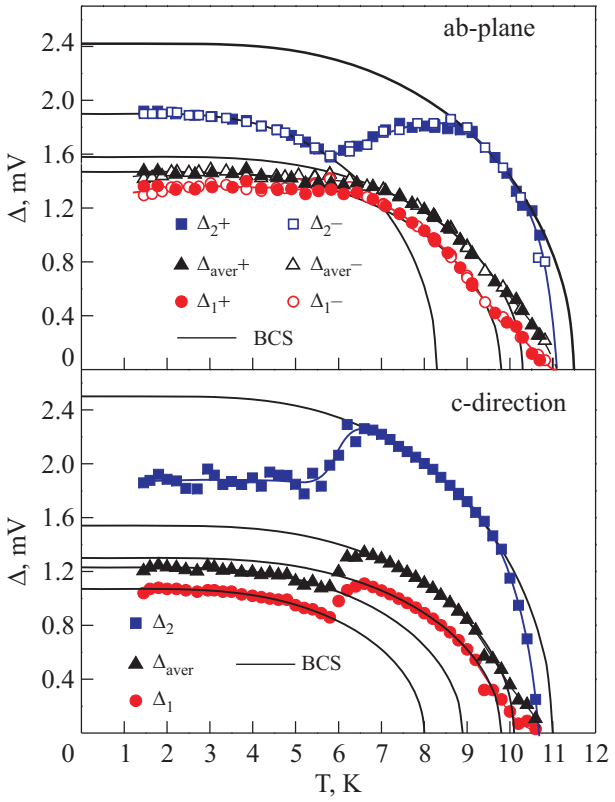

Fig. 11. Temperature dependencies of gaps Δ (GBTK [21]) calculated in the two-gap approximation by Eq. (2) for the PC in Fig. 1. The average gaps are $\Delta_{aver} = \Delta_1 K + \Delta_2(1-K)$. The polynomial fit runs through the points outside the BCS approximations. The scaling factors are $S_{ab} = 0.35$ and $S_c = 0.5$. The contribution to conductivity from the smaller gap is $K = 0.8$ (K = const).

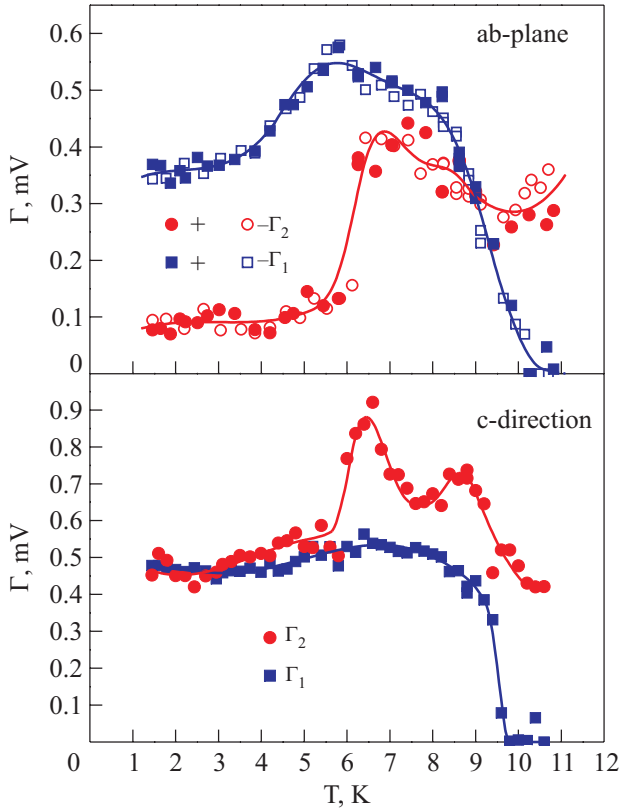

Fig. 12. Temperature dependencies of broadening parameters Γ calculated in the two-gap GBTK model. Γ_2 and Γ_1 are for the larger (Δ_2) and smaller (Δ_1) gaps, respectively (Fig. 11). For clarity, a polynomial fit is drawn through the points.

high-energy part of the gap is important in the one-gap approximation. The temperature dependencies of gaps and broadening parameters discussed in this section are of illustrative character because of K = const. The goal was to show that they have different shapes and T_c differs from BCS extrapolated critical temperatures. Note that the average gaps shown in this figure practically coincide with those calculated in the one-gap approximation (Fig. 5).

BB model

The two-band approximation in the BB model was considered in [19] using a free scaling factor S. Here we report the results obtained with a fixed scaling factor ($S = 0.25$) for both directions (see Appendix B and Fig. 20,*c*,*d*). In contrast to the GBTK approximation, the contribution K of the smaller gap to conductivity was not constant. Nevertheless the number of fitting parameters was the same because at $T > 2$ K γ_1 turns zero in both directions and hence is no longer a fitting parameter. Besides, unlike the broadening parameter Γ, the pair-breaking parameter γ does not increase the uncertainty in calculating the rms deviation (cf. Fig. 18 with free S and Fig. 19, Appendix B).

The temperature dependencies of the larger Δ_2, smaller Δ_1 and the average OP Δ_{aver}, Eq. (3), are shown in Fig. 13.

Note that the use of another model and a non-fixed K to conductivity affect the behavior of the temperature dependencies of the OPs (mainly the smaller OP) in comparison to the GBTK model and BB approximation with varying S [19]. In the *ab*-plane the smaller OP decreases rapidly with temperature and the BCS extrapolation gives $T_c \sim 3.3$ K. At $T > 3$ K Δ_1 in the AFM region changes into the BCS dependence with $T_c \sim 6.15$ K. In the PM region there is a region of a smoothly decreasing gap which persists up to the normal state. This region may be due to the interband interaction. In the *c*-direction the BCS extrapolated T_c values for Δ_1 are somewhat higher: ~ 4.8 K (AFM region) and ~ 8 K (PM region).

The temperature dependencies of the larger OP Δ_2 especially in the PM region closely resemble the shapes of the curves for the OP calculated in the one-gap approximation within the BB model with a varying scaling factor (Fig. 9). The reason for the coincidence is quite obvious. In the PM region the shape of the curve is mainly dependent on the larger OP because its value is several times higher

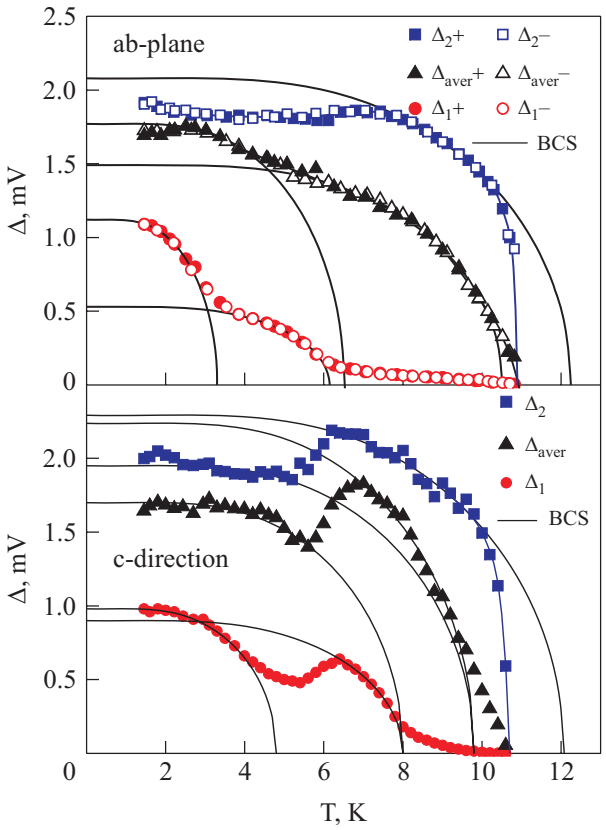

Fig. 13. Temperature dependencies of OPs Δ (BB model [20]) calculated in the two-gap approximation by Eq. (2) for the PC in Fig. 1. The polynomial fit is drawn through points outside the BCS approximation. $S = 0.25$ in both cases.

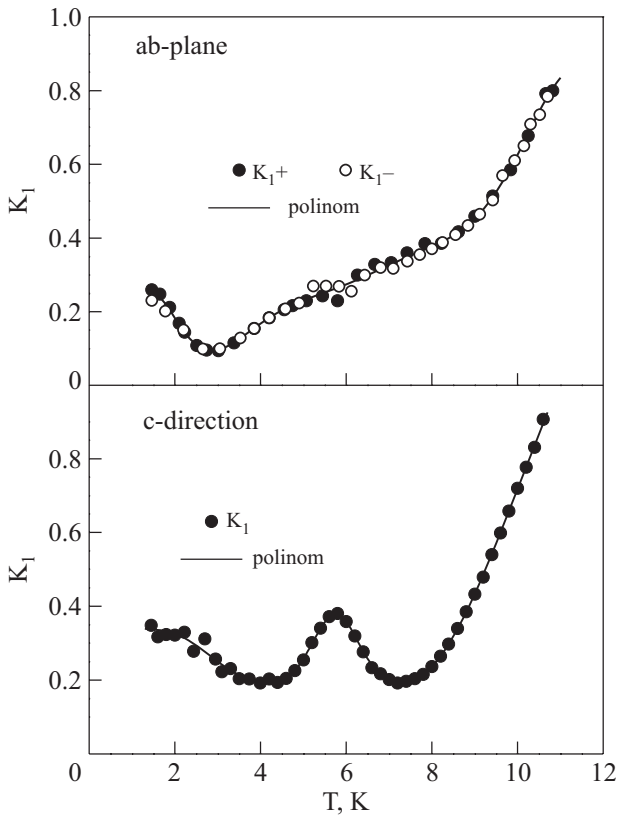

Fig. 14. Temperature dependencies of the contribution to conductivity from the smaller OP (Fig. 15) calculated in the two-gap BB model.

than that of the smaller OP. In contrast to the one-gap approximation, the contribution of the smaller OP to the conductivity holds the scaling factor S constant. Since in the low temperature region OPs of different bands are comparable in magnitude, the distinctions between the larger OP of two-band calculations and the OP in the one-gap approximation are more explicit in the shapes of the curves. The critical temperatures obtained by BCS extrapolation for Δ_2 in the PM region practically coincide with the one-gap calculation ($T_c \sim 12$ K) and exceed the superconducting transition temperature of the compound. On approaching $T \sim 10$ K the OPs start to depart from the BCS dependence tending to 0 at T_c of the sample. It is interesting that the temperature dependencies of the average OP Δ_{aver} have sections in both directions in the PM region that decrease almost linearly and go through zero at T_c of the sample.

Let us consider the temperature-dependent contribution K to conductivity made by the smaller gap (Fig. 14 and Eq. (2)).

At low temperatures the dependence $K(T)$ is readily predictable qualitatively: K decreases with a decrease in Δ_1. On a further rise of temperature these parameters exhibit a correlated change in the *c*-direction: the growth of Δ_1 due to the reduced influence of spin density waves is attended with an increase in K. The somewhat different degrees of the changes in these parameters in the *c*-direction and the absence of a similar correlation in the *ab*-plane might be attributed to the increasing pair-breaking parameter for Δ_2 (Fig. 15) but this assumption is in conflict with the sharp growth of K in PM region. It is then, reasonable to assume that K grows because the relative share of the FS containing the large gap decreases. This fact can be explained as follows.

It is pointed above that the scaling factor S is dependent in particular on what part of the whole FS is occupied by superconductivity. If $S = \text{const}$., this share is independent of temperature. Also, the areas of the FS bands that contain a larger and a smaller gap are also temperature-independent. This suggests that if the FS area with a large OP decreases, superconductivity in this part of the band is not suppressed fully. In terms of our assumption, the OP in the «vacant» part of the band reduces and becomes comparable to the OP in the second zone. We may thus conclude that the superconducting share of the total FS area remains invariable. This can account for the redistribution of the relative FS shares between the large and small OPs. Near T_c on approach of $T \sim 10$ K the contribution of the large OP to conductivity falls below $\sim 20\%$. As a result, Δ_2 deviates from the BCS dependence and turns rapidly to zero. The

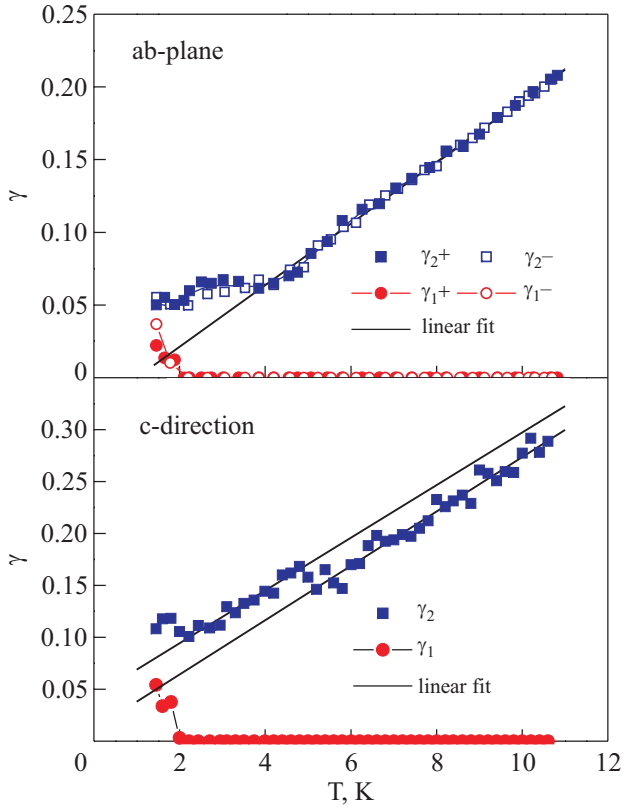

Fig. 15. Temperature dependencies of the pair-breaking parameter γ calculated in the two-gap BB model. γ_2 and γ_1 correspond to the larger OP (Δ_2) and to the smaller OP (Δ_1) respectively (Fig. 13). For clarity, a linear fit is drawn through the points.

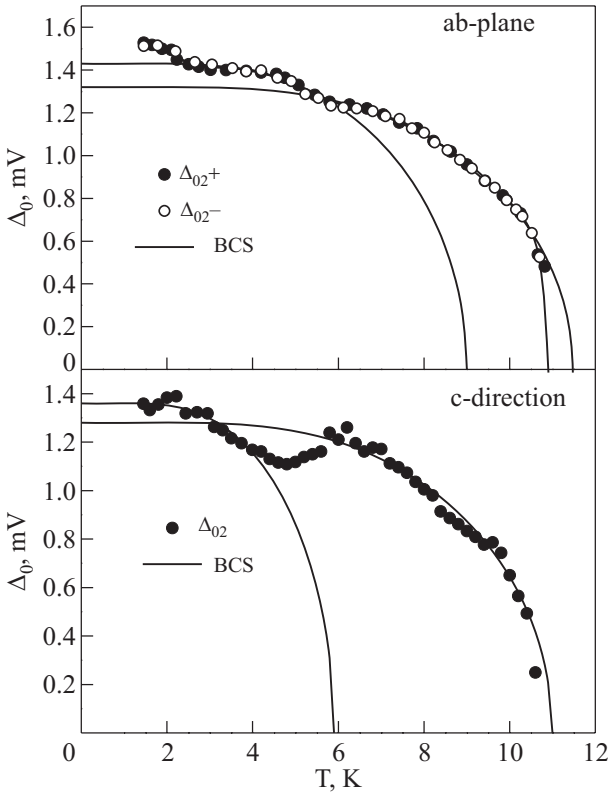

Fig. 16. The temperature dependence of the lager gap $\Delta_{02} = \Delta_2(1-\gamma_2^{2/3})^{3/2}$ (BB model) for the $ErNi_2B_2C$–Ag PC in the *ab*-plane and the *c*-direction (Fig. 13). Solid lines are BCS extrapolations. Since $\gamma_1 = 0$, the smaller gap behaves similarly to the small OP.

physical reason for the reduction of the FS area with a large OP may be connected with the spin fluctuations which enhance with temperature. It is likely that larger OP occurs in the FS part less protected by the presence of the localized rare-earth magnetic moments. This assumption is supported by the values of pair-breaking parameters γ_2 of large OP which increase with temperature. Note that the γ_2 magnitudes of larger OP calculated in the two-gap approximation within the BB model for nonmagnetic $LuNi_2B_2C$ are lower and decrease (faster in the *ab*-plane) with temperature (see [23], Fig. 9). Since spin–flip scattering is absent in this compound, the parameter γ in this calculation tends to exceed the degree of the superconducting gap broadening. Note that in $YNi_2B_2C$the gap is most broadened in the low-energy part ([29], Fig. 6). Assuming that this reasoning holds for $ErNi_2B_2C$ too, we can conclude that no broadening of larger and smaller gaps occurs above 2 K (Fig. 15) where the parameter γ is determined solely by the processes of scattering at magnetic moments. It is therefore most justified to apply the two-gap modification of the BB model in this case. The temperature dependencies of broadening parameters γ are shown in Fig. 15. Two practically parallel parts of a linear growth of γ_2 in the AFM and PM regions are distinctly seen in the *c*-direction. There is only one linear portion in the *ab*-plane, which may indicate that spin-density waves are ineffective during a magnetic transition. Note that the illustrated curves correlate to a certain degree with the curves describing the contribution of a smaller OP to conductivity (Fig. 14).

Figure 16 illustrates the temperature dependence of the energy gap Δ_0 corresponding to Δ_2 of the larger OP. There are different BCS extrapolations for changing to gapless superconductivity in the AFM (9 K and ~ 6 K in the *ab*-plane and *c* -direction, respectively) and PM (~11 K in both directions) regions. The gap, like the OP, grows during the transition to the PM state in the *c*-direction and has a monotonic dependence in the a*b*-plane.

It is interesting that the tunnel parameter Z (Fig. 17) has a feature at T_N only in the *c*-direction, like in the one-gap case (Fig. 9), which may be attributed to the effect of spin-density waves.

Conclusions

A detailed analysis of the temperature dependencies of PC Andreev reflection spectra $dV/dI(V)$ has been performed for $ErNi_2B_2C$ ($T_c \approx 11$ K) in the *ab*-plane and *c*-di-

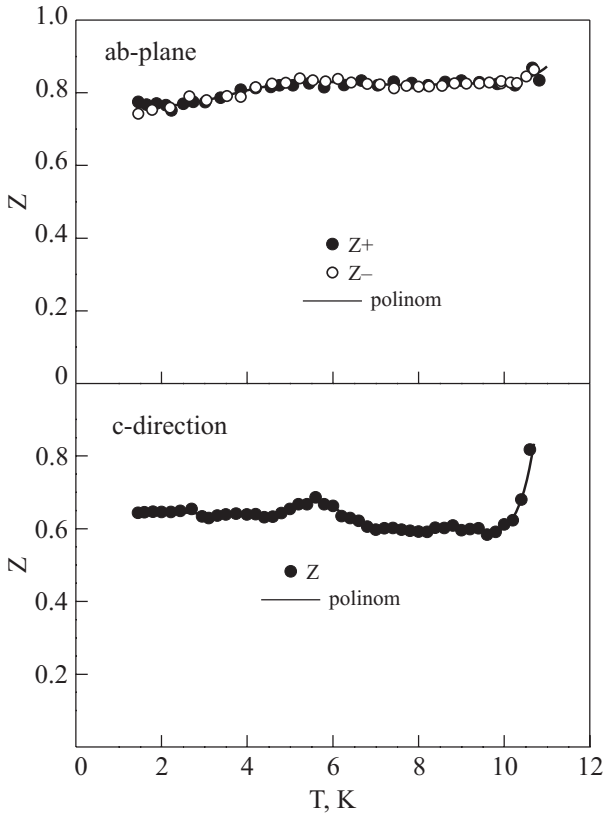

Fig. 17. Temperature dependencies of the tunnel parameter Z (two-gap BB approximation for the $ErNi_2B_2C$–Ag PC in the *ab*-plane and the *c*-direction).

rection using one-gap and two-gap approximations. Two models were used: the traditional GBTK model including the broadening parameter Γ [21] and the BB model [20] in which the parameter γ characterizes the pair-breaking effect of magnetic moments (likely Er). For the first time the calculation has been made comparing both the shape and the intensity of experimental and theoretical curves. This has decreased the degree of uncertainty in the temperature dependence $\Delta(T)$ for contacts with high broadening parameters Γ.

The following conclusions have been drawn.

1. An anisotropic effect of AFM ordering has been detected irrespective of the data processing model. For example, the magnitude of the superconducting gap calculated within the one-gap GBTK model decreases on transition to the AFM state by $\sim$ 25% in the *c*-direction and by $\sim$ 4–7% in the *ab*-plane, which correlates with the behavior of the averaged gap in the two-gap approximation within the BB model [19].

2. The intensity of the PC spectra $dV/dI(V)$ changes in correlation with the gap: the intensity decreases monotonically in the *ab*-plane and has an extremum near the AFM transition in the *c*-direction. This behavior may be due to the orientation-dependent pair-breaking effect of spin-density waves. Thus it has been found unambiguously that the AFM transition has an anisotropic effect on the superconducting state.

3. As in [19], the pair-breaking parameter γ increases in the vicinity of magnetic transitions, which is natural to attribute to the effect of spin fluctuations under a change of the magnetic order.

4. It has been shown that the proper choice of the scaling factor S in the one-gap GBTK calculation gives the ratio $2\Delta(0)/kT_c \sim 3.52$ for the gap in the PM region and its BCS like temperature dependence. The ratio obtained in the one-gap calculation within the BB model is $2\Delta(0)/kT_c \sim 4.08–5.14$.

5. The analysis of the models shows that the two-gap calculation in the BB model with a fixed scaling factor S provides the most adequate information. This calculation gives different BCS extrapolation data for T_c of the larger and smaller OPs, which points to the multiband nature of superconductivity in $ErNi_2B_2C$. Its physical sense is that there are FS parts with a weaker electron–phonon interaction (EPI) in which the temperature induced suppression of superconductivity is faster. This is supported by the calculation of the anisotropy of the EPI parameter in $LuNi_2B_2C$ [4], which can vary from 0.3–0.8 on a spheroidal FS to 1.0–2.7 on a cube-like FS.

Acknowledgement

Work at Texas A&M University was supported by the Robert A. Welch Foundation, Houston Texas (Grant A-0514) and work in ILTPE was supported by NAS of Ukraine.

Appendix A: Some details of calculation technique

The technique used (detailed in [23]) is based on a selection of parameters that can ensure the smallest rms divergence between experimental and theoretical curves. First, the curves $dV/dI(V)$ were normalized to the curve $dV/dI(V)$ taken above T_c and symmetrized. The curve fitting was performed in the interval ± 8 mV to avoid the effect of the phonon features (inflection points) in the vicinity of 10 mV in some curves (see Fig. 1).

Appendix B: Choice of proper scaling factor S

Theoretically $S = 1$. But $S < 1$ happens very often too. The reasons may be as follows.

1. The electron transport through a PC deviates from the ballistic conditions [39].

2. An inhomogeneity at which the PC region at the *S*-electrode side is not fully superconducting because of the normal region (regions) near the NS boundary in the superconductor.

3. A superconducting gap can occur only in a part of the FS. For example, the AFM molecular field induces a gap in some FS parts in $ErNi_2B_2C$ and suppresses the superconducting gap in these regions.

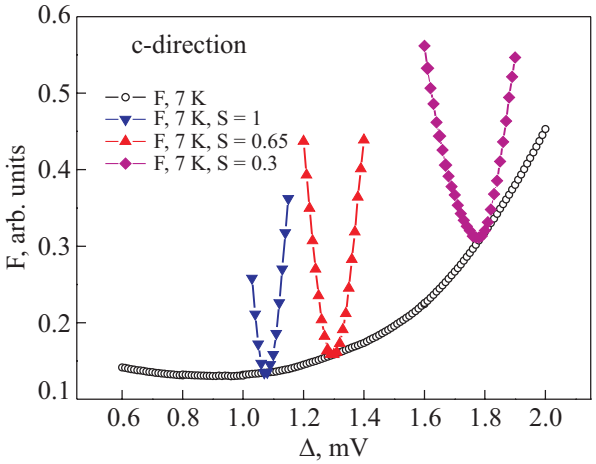

Fig. 18. The dependence of the rms deviation F of the shape of the theoretical curve from experimental Δ at 7 K in the *c*-direction. The intensity ratio $S = (dV/dI(V))_{\text{exp}}/(dV/dI(V))_{\text{theor}}$ between experimental and theoretical curves is changing from 3.58 to 0.23 The lowest F corresponds to the best coincidence of the experimental and theoretical curves is obtained at $\Delta = 0.96$ meV and $S = 1$.The narrow parabolic error curves were taken at $S = \text{const}$ (one-gap GBTK model [21].

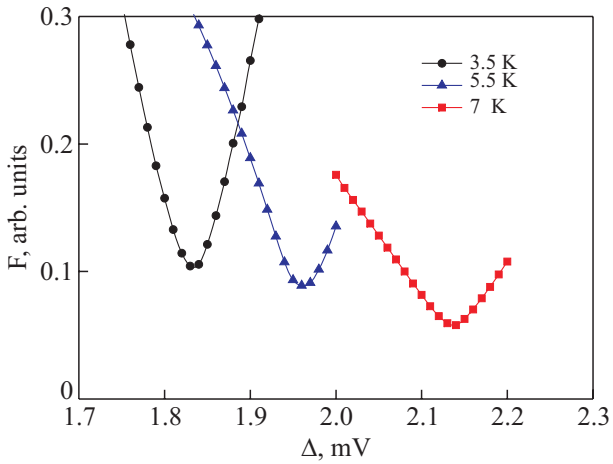

Fig. 19. The dependence of the mutual rms deviation F of the theoretical and experimental curve shapes from Δ (BB model) in the *c*-direction at different temperatures. S varies along the curves and at the minima, $T = 3.5$, 5.5, and 7 K, being $S =$ = 0.24, 0.2, and 0.22, respectively.

A more exotic case of $S > 1$ is also possible. For example, to improve the description of the shapes of smeared experimental curves, the parameter Γ which assumes a finite lifetime of carriers is usually increased. As a result, the intensity of theoretical curves decreases. However, if the spectra $dV/dI(V)$ are smeared e.g., because of different values (distribution) of the superconducting gap in different FS parts due to anisotropy or multiband superconductivity, the theoretical Γ-broadening curve can approach the shape of the experimental curve, but its intensity will be lower, and the scaling factor S can exceed 1. This can be used as a criterion of validity for a model. As an example, we consider the spectrum from Fig. 14 in [24]. The gap is distributed in the interval 1–3.35 meV (insert). The calculation in [23] gives:

1. GBTK (1-gap): $\Delta = 2.565$ meV, $\Gamma = 0.523$ meV, $Z = 0.8$, $S = 1.467$.

2. GBTK (2-gaps): $\Delta_1 = 2.18$ meV; $\Delta_2 = 2.99$ meV; $\Gamma_1 = 0.36$ meV; $\Gamma_2 = 0.067$ meV; $Z = 0.78$; $K = 0.56$; $\Delta_{\text{aver}} = 2.538$ meV; $S = 1.144$.

3. BB (1-gap): $\Delta = 2.79$ meV, $\gamma = 0.04$, $Z = 0.74$, $S = 0.968$.

4. BB (2-gaps): $\Delta_1 = 2.15$ meV; $\Delta_2 = 2.984$ meV; $\gamma_1 = 0.046$; $\gamma_2 = 0.011$; $Z = 0.75$; $K = 0.315$; $\Delta_{\text{aver}} =$ = 2.72 meV; $S = 0.968$.

Thus, the one-gap GBTK calculation results in the highest value in the S estimate. Therefore one-gap GBTK calculations [40] can be regarded as oversimplified and can be used only as a first approximation. In ordinary superconductors, e.g., Zn [41], $S \approx 1$ is independent of temperature because the gap opened isotropically on the whole FS at $T < T_c$.

In Fig. 18 the smooth broad arc-like curve corresponds shows rms deviation of the shapes of theoretical and experimental curves for the gap Δ in the interval 0.6–2 meV. The lowest error is at $\Delta = 0.96$ meV. The scaling factor varies along the curve from $S = 3.58$ at $\Delta = 0.6$ meV to $S = 0.23$ at $\Delta = 2$ meV and $S = 1.3$ at the minimal F. $S > 1$ is possible only assuming the gap distribution (see above), and therefore the *lowest* F *(shape error) alone is not sufficient to be a criterion*. Besides, for the curves taken at higher Γ values a comparatively small change in the shape of the temperature-neighboring curves $dV/dI(V)$ can shift arbitrarily the error minimum and the corresponding Δ.

Unlike the GBTK model, the error curves obtained in the BB model have distinct minima (Fig. 19). In our case the criterion of the proper choice of the scaling factor S was its value at which the shapes of the theoretical and experimental curves coincided most closely in the whole interval of temperatures used. To avoid overloading, Fig. 20 contains the F and S calculation for two characteristic temperatures: $T = 3.5$ K in the middle of the AFM region and $T = 7$ K, i.e., above the temperature of AFM ordering. It follows from Fig. 20 that S can vary from 1 to 0.2, being the lowest at $\Gamma \to 0$ (Fig. 20). The vertical lines show the best *S*-values corresponding to the minimum error along with their associated gaps (OPs) and broadening (pair-breaking) parameters. Note that in the BB model a departure from the best-chosen *S*-value caused a sharp increase in the error *F*, and therefore the limits of *S* variation are rather narrow. On the other hand, the GBTK

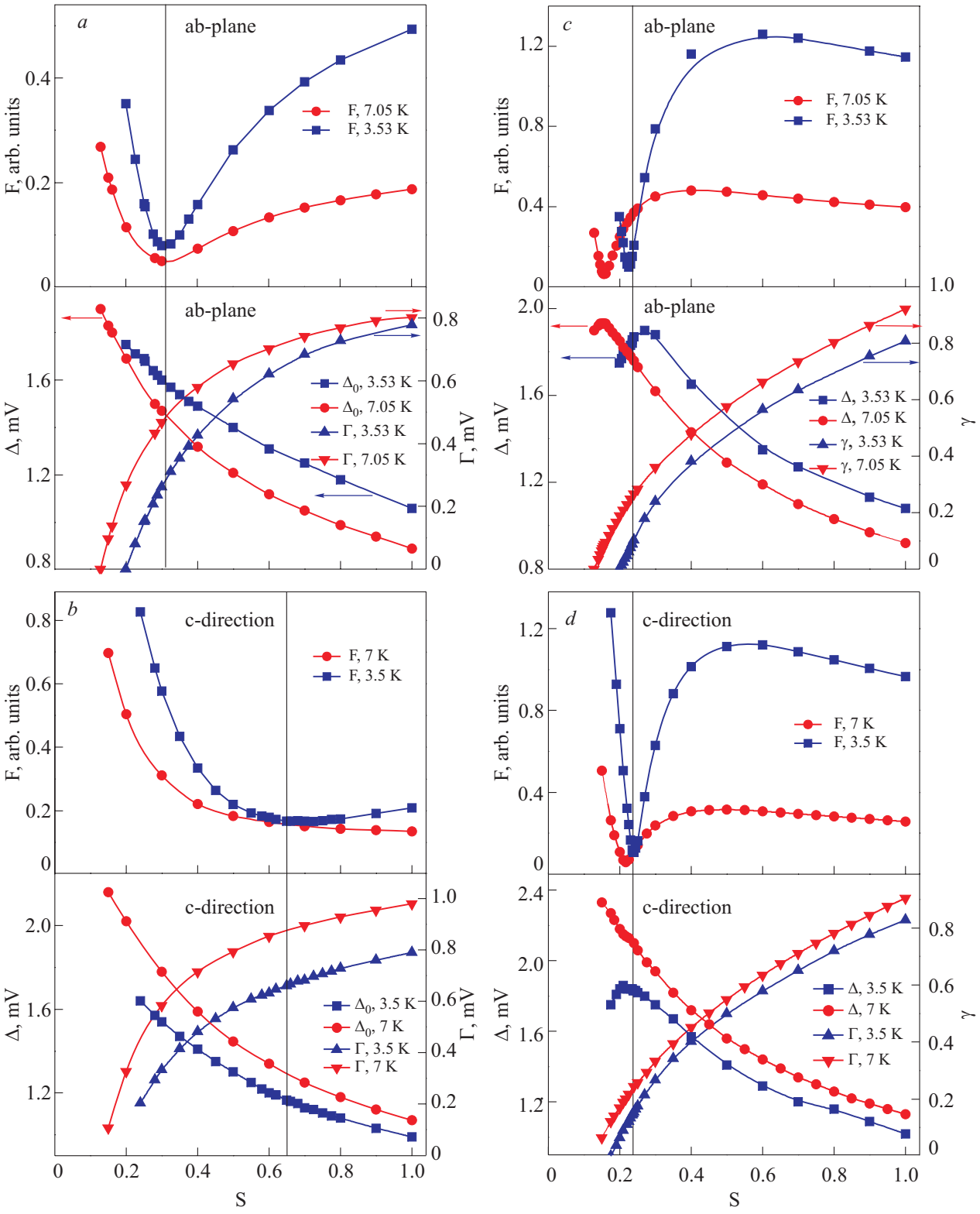

Fig. 20. Dependence of the relative deviation of the shapes F of theoretical and experimental curves from S calculated in the GBTK (*a*,*b*) and BB (c,d) models at $T = 3.5$ K and 7 K in the *ab*-plane and in the *c*-direction. The lower part of each figure shows the corresponding dependencies of the gap (OP) Δ and the broadening Γ (pair-breaking γ) parameters. The vertical line marks the best choice of S corresponding to the closest coincidence of the curve shapes at both temperatures

model [21] allows more freedom of selecting *S*, especially in the *c*-direction. However, this variation has practically no effect on the shape of temperature dependence $\Delta(T)$ because the curves $\Delta(S)$ are nearly parallel at both temperatures. The gap can be estimated readily at another S value using the dependence $\Delta(S)$.

Appendix C: One-gap BB calculation with S ≠ const

Unlike the GBTK model, the $F(\Delta)$ curves obtained in the BB model have distinct minima (Fig. 19). Using a fixed S impairs considerably the quality of fitting in this approximation. The results of the one-gap calculation allowing for the minima in the curves are illustrated in Fig. 9 and the dependencies $S(T)$ are shown in Fig. 3. The decrease in the *S*-value is due to the two-gap character of superconductivity in this compound, which determines different OP magnitudes and a different (in comparison to the GBTK result) shape of the density of states. The relative share of the FS with a larger OP decreases at rising temperature (see the Two-gap BB calculation section). Used in BB theory the density of states terminates abruptly at the gap edge. In the one-gap approximation of the experimental curve this entails termination of the contribution to conductivity from the FS parts with smaller OPs. However, since the spectrum intensity is estimated assuming that the OP obtained is related to the whole Fermi surface, S decreases. The difference between the dependencies $S(T)$ in the *c*-direction and the *ab*-plane can be attribute to the anisotropic effect of spin-density waves (see the above interpretation of the quantity M and Fig. 3). The temperature-dependent AFM molecular field induces a gap in some parts of FS in the *c*-direction and destroys the superconducting gap in them. An AFM gap is more probable in the FS parts which have a smaller superconducting gap taking into account the temperature dependence of the OP in the corresponding temperature region.

The sharp decrease in the OP on approaching T_c can also be caused by the two-band structure of the FS and the reduction of the FS share with a larger OP. There may exist a certain minimal FS share with a large OP below which superconductivity is destroyed rapidly due to the interband interaction. In our case the departure from the BCS dependence started in both directions at $T \sim 10$ K at which the contribution of the larger OP to conductivity dropped below 20% (two-gap calculation).

Appendix D: Reducing the number of fitting parameters for the two-gap GBTK model

As noted in the Introduction, in the general case the two-gap calculation by Eq. (2) involves seven fitting parameters (Δ_1, Δ_2, Γ_1, Γ_2, Z, S and K). This has an unfavorable effect on the estimates obtained. It is therefore desirable to minimize the number of such parameters on the basis of physically reasonable limitations. In the strict sense, the scaling factor S is not a fitting parameter. It does not enter into the theoretical formulas describing current-voltage characteristics. It is intended to equalize the intensities of experimental and theoretical curves on calculating the mutual rms deviation of their shapes. However, a use of S = const restricts the range of permissible values for the rest of the fitting parameters. A fixed S reduces the number of fitting parameters at least by one parameter (Fig. 18). We did not fix the tunnel parameter Z which was found to be approximately constant except near T_c. As a result, we have four fitting parameters instead of seven. Besides, it is reasonable to fix the relative contribution K to conductivity from each band.

Thus, the calculation was made using fixed $S = 0.35$ in the *ab*-plane and $S = 0.5$ in the *c*-direction. The relative contribution of the smaller gap to conductivity was $K = 0.8$ in both directions. Fixed K actually couples Δ and Γ, which can distort their temperature dependencies. Indeed, if, for example, the first gap remains constant and the second one decreases, the relative contribution of the first gap increases (it is assumed that the FS share of each gap does not change). To exclude this, it is necessary to decrease the broadening parameter of the second gap or to increase it for the first one. Identical temperature dependencies for gaps and broadening parameters is the simplest version free of distortions.

Note added in proof

After the paper was sent to arXiv, we were aware about recent three-dimensional study of the Fermi surface of $LuNi_2B_2C$ in [42]. This study shows that (i) the Fermi surface topology of the rare-earth nickel borocarbides varies little for rare-earth elements such as Er, Tm and Yb, (ii) there are 3 bands which contribution to the density-of-states (DoS) at the Fermi energy is 0.24%, 22.64% and 77.1%. That is, two bands basically contribute to DoS and therefore our two-band approach is reasonable.

1. K.-H. Müller and V.N. Narozhnyi, *Rep. Prog. Phys.* **64**, 943 (2001).
2. K.-H. Müller, M. Schneider, G. Fuchs, and S.-L. Drechsler, *Handbook on the Physics and Chemistry of Rare Earths*, A. Karl, Jr. Gschneidner, Jean-Claude Bünzli, and Vitalij K. Pecharsky (eds.), North-Holland, Elsevier (2008), v. 38, p. 175.
3. L.C. Gupta, *Adv. Phys*. **55**, 691 (2006).
4. B. Bergk, V. Petzold, H. Rosner, S.-L. Drechsler, M. Bartkowiak, O. Ignatchik, A.D. Bianchi, I. Sheikin, P.C. Canfield, and J. Wosnitza, *Phys. Rev. Lett.* **100**, 257004 (2008).
5. S.-L. Drechsler, S.V. Shulga, K.-H. Müller, G. Fuchs, J. Freudenberger, G. Behr, H. Eschrig, L. Schultz, M.S. Golden, H. von Lips, J. Fink, V.N. Narozhnyi, H. Rosner, P. Zahn, A. Gladun, D. Lipp, A. Kreyssig, M. Loewenhaupt, K. Koepernik, K. Winzer, and K. Krug, *Physica* **C17–318**, 117 (1999).
6. S.V. Shulga, S.-L. Drechsler, G. Fuchs, K.-H. Müller, K. Winzer, M. Heinecke, and K. Krug, *Phys. Rev. Lett.* **80**, 1730 (1998).
7. G. Goll, M. Heinecke, A.G. M. Jansen, W. Joss, L. Nguyen, E. Steep, K. Winzer, and P. Wyder, *Phys. Rev.* **B3**, R8871 (1996).
8. L.H. Nguyen, G. Goll, E. Steep, A.G. M. Jansen, P. Wyder, O. Jepsen, M. Heinecke, and K. Winzer, *J. Low Temp. Phys.* **105**, 1653 (1996).

9. C. Detlefs, A.H. M.Z. Islam, T. Gu, A.I. Goldman, C. Stassis, P.C. Canfield, J.P. Hill, and T. Vogt, *Phys. Rev.* **B6**, 7843 (1997).
10. V.D. Fil', *private communication*.
11. E.E. M. Chia, M.B. Salamon, T. Park, H.-J. Kim, S.-I. Lee, and H. Takeya, *Europhys. Lett.* **73**, 772 (2006).
12. L.F. Rybalchenko, I.K. Yanson, A.G.M. Jansen, P. Mandal, P. Wyder, C.V. Tomy, and D.McK. Paul, *Physica* **B18**, 189 (1996).
13. T. Watanabe, K. Kitazawa, T. Hasegawa, Z. Hossain, R. Nagarajan, L. Watanabe, and C. Gupta, *J. Phys. Soc. Jpn.* **69**, 2708 (2000).
14. I.K. Yanson, in: *Rare Earth Transition Metal Borocarbides (Nitrides): Superconducting, Magnetic and Normal State Properties*, K.-H. Müller and V.N. Narozhnyi (eds.), Kluwer Academic Publishers, The Netherlands (2001).
15. M. Crespo, H. Suderow, S. Vieira, S. Bud'ko, and P.C. Canfield, *Phys. Rev. Lett.* **96**, 027003 (2006).
16. T. Baba, T. Yokoya, S. Tsuda, T. Kiss, T. Shimojima, K. Ishizaka, H. Takeya, K. Hirata, T. Watanabe, M. Nohara, H. Takagi, N. Nakai, K. Machida, T. Togashi, S. Watanabe, X.-Y. Wang, C.T. Chen, and S. Shin, *Phys. Rev. Lett.* **100**, 017003 (2008); T. Baba, T. Yokoya, S. Tsuda, T. Kiss, T. Shimojima, K. Ishizaka, H. Takeya, K. Hirata, N. Nakai, K. Machida, T. Togashi, C.T. Chen, C.Q. Zhang, S. Watanabe, and S. Shin, *Physica* **C69**, 928 (2009).
17. R.C. Dynes, V. Narayanamurty, and J.P. Garno, *Phys. Rev. Lett.* **21**, 1509 (1978).
18. K. Machida, K. Nokura, and T. Matsubara, *Phys. Rev.* **B2**, 2307 (1980).
19. N.L. Bobrov, V.N. Chernobay, Yu.G. Naidyuk, L.V. Tyutrina, D.G. Naugle, K.D.D. Rathnayaka, S.L. Budko, P.C. Canfield, and I.K. Yanson, *Europhys. Lett.* **83**, 37003 (2008).
20. S.I. Beloborod'ko, *Fiz. Nizk. Temp.* **29**, 868 (2003) [*Low Temp. Phys.* **29**, 650 (2003)].
21. A. Plecenik, M. Grajcar, P. Seidel, and A. Pfuch, *Phys. Rev.* **B1**, 16185 (1995).
22. X.Y. Miao, S.L. Bud'ko, and P.C. Canfield, *J. Alloys and Compounds* **338**, 13 (2002).
23. N.L. Bobrov, S.I. Beloborod'ko, L.V. Tyutrina, V.N. Chernobay, I.K. Yanson, D.G. Naugle, and K.D.D. Rathnayaka, *Fiz. Nizk. Temp.* **32**, 641 (2006) [*Low Temp. Phys.* **32**, 489 (2006)].
24. N.L. Bobrov, S.I. Beloborod'ko, L.V. Tyutrina, I.K. Yanson, D.G. Naugle, and K.D.D. Rathnayaka, *Phys. Rev.* **B1**, 014512 (2005).
25. B.N. Engel, G.G. Ihas, E.D. Adams, and C. Fombarlet, *Rev. Sci. Inst.* **55**, 1489 (1984).
26. S. Skanthakumar and J.W. Lynn, *Physica* **B59–261**, 576 (1999).
27. G.E. Blonder, M. Tinkham, and T.M. Klapwijk, *Phys. Rev.* **B5**, 4515 (1982).
28. T. Claeson, in: *Tunneling Phenomena in Solids*, E. Burstein and S. Lundquist (eds.), Plenum Press, New York (1969).
29. H. Nishimori, K. Uchiyama, Sh. Kaneko, A. Tokura, H. Takeya, K. Hirata, and N. Nishida, *J. Phys. Soc. Jpn.* **73**, 3247 (2004).
30. M.L. Kulic, J. Keller, and K.D. Schotte, *Solid State Commun.* **80**, 345 (1991).
31. J.P. Brison, P. Lejay, A. Buzdin, and J. Flouquet, *Physica* **C229**, 79 (1994).
32. Yu.G. Naidyuk, H. von Löhneysen, G. Goll, I.K. Yanson, and A.A. Menovsky, *Europhys. Lett.*, **33**, 557 (1996).
33. E.E.M. Chia, W. Cheong, Tuson Park, M.B. Salamon, Eun-Mi Choi, and Sung-Ik Lee, *Phys. Rev.* **B72**, 214505 (2005).
34. H. Chi and A.D.S. Nagi, *J. Low Temp. Phys.* **86**, 139 (1992).
35. P.L. Gammel, B.P. Barber, A.P. Ramirez, C.M. Varma, D.J. Bishop, P.C. Canfield, V.G. Kogan, M.R. Eskildsen, N.H. Andersen, K. Mortensen, and K. Harada, *Phys. Rev. Lett.* **82**, 1756 (1999).
36. K. Maki, H. Won, and S. Haas, *Phys. Rev.* **B9**, 012502 (2004).
37. V.L. Pokrovsky, *Zh. Eksp. Teor. Fiz.* **40**, 641 (1961).
38. V.L. Pokrovsky and M.S. Ryvkin, *Zh. Eksp. Teor. Fiz.* **43**, 92 (1962).
39. I.N. Askerzade and I.O. Kulik, *Mod. Phys. Lett.* **B17**, 649 (2003).
40. X. Lu, W.K. Park, S. Yeo, K.-H. Oh, S.-I. Lee, S.L. Bud'ko, P.C. Canfield, and L.H. Greene, *arXiv:1004.3846*.
41. Yu.G. Naidyuk, H. von Löhneysen, and I.K. Yanson, *Phys. Rev.* **B4**, 16077 (1996).
42. S.B. Dugdale, C. Utfeld, I. Wilkinson, J. Laverock, Zs. Major, M.A. Alam, and P.C. Canfield, *Supercond. Sci. Technol.* **22**, 014002 (2009).